Sinc-Function-Based Friction Compensation for Ball-Screw-Driven Stage in Zero-Velocity Region including Non-Velocity-Reversal motion

Hongzhong Zhu*, Hiroshi Fujimoto (The University of Tokyo)

Abstract

This paper presents a heuristic friction compensation approach for handling the rolling friction behaviors of ball-screw-driven stages in the zero-velocity crossing regions including non-velocity-reversal motion. The rolling friction behaves in a nonlinear way, and would significantly deteriorate the control performance. Since the alteration of elastic energy in mechanical components of a stage system is different between the velocity-reversal motion and non-velocity-reversal motion, sophisticated compensation approaches become necessary to cope with the both cases. In this study, a velocity pattern recognition algorithm is proposed as the first step in the design process to classify the velocity patterns in zero-velocity crossing region. Then, sinc function is utilized to model the nonlinear rolling friction of the ball-screw-driven stage. Thanks to the few parameters of the sinc function, it is possible to approximately compute the released displacement in the non-velocity-reversal motion, and the friction compensation approach can therefore be applied in a feedforward manner. It is verified by experiments that the proposed approach can precisely compensate the nonlinear friction to improve the control performance.

Key words: nonlinear friction compensation, motion control, zero velocity crossing motion, sinc function, disturbance observer, ball-screw-driven stage

1. Introduction

Ball screws are linear actuators that translate rotational motion to linear motion with little friction and high efficiency, and are extensively used in industrial equipments. As the fast and precise positioning/servo control is increasingly required to improve the productivity, controllers with higher robustness become necessary [1] [2]. Due to the nonlinear characteristics of the rolling friction which originates at elastic deformation of the mechanical components, the control performance may be significantly degraded at low speed motion, especially at the zero velocity crossing motion, such as the so-called quadrant glitch phenomenon [3].

In order to compensate the nonlinear friction, many research groups concentrated on developing accurate friction models. Dahl proposed a dynamic model which can explain the spring-like behavior in stiction [6]. LuGre model, which is an extension of the Dahl model, can capture more static and dynamic properties of friction [4]. Swevers *et al.* also presented a complete and accurate model that can describe the hysteresis characteristics of the friction [7]. Though the effectiveness of these models were reported in the literature, they are too complex to construct and the advanced knowledge on the determination of parameters is required, which limits their application. In order to take more priority over the ease of implementation, a heuristic friction model, which is also referred to the Generalized Maxwell-Slip Model (GMS), was proposed [5]. However, the model also has many parameters that should be precisely identified, which is also a time consuming task. In addition, most of the proposed approaches only considered the compensation at the velocity reversal case, which may not enough for complex machining. For instance, if the stage is decelerated to zero velocity and then accelerated in the same direction, the friction characteristics would be quite different from the case of reversal motion since the elastic energy stored in the mechanical components is not fully released.

In general, friction characteristics of ball-screw-driven stages varies according to the drive conditions, operation environments, and so on. Model-based friction compensation approaches usually cannot adjust themselves to adapt for new situations. In order to cope with these problems, some repetitive learning approaches were proposed [12] [13]. The approaches provide a good option for us if the contour is determined and repeated within a short period. However, if this is not the case, say, the trajectory is complicated and non-periodic, these approaches are not applicable.

Another well known approach for suppressing disturbance including nonlinear friction in motion control is the disturbance observer [8]. However, due to the phase lag of the introduced low-pass filter and the inaccuracy of velocity signal at low speed motion, the effects caused by friction at zero velocity cannot be completely suppressed. Because of this reason, disturbance observer method and friction compensator coexist in many proposed approaches [3] [10]. We also apply this structure in this study.

In this paper, a velocity pattern classification at zero velocity crossing region is first presented. Based on the velocity patterns, a heuristic approach of friction compensation for ball-screw-driven stage is proposed using sinc function. It is demonstrated that the rolling friction characteristics can be properly fitted by sinc function. The potential advantages of using sinc function are that there are only two parameters needed to be designed and it is also possible to calculate the inverse function, which can be utilized for friction compensation at the non-velocity-reversal motion. In addition, the

Table 1. Parameters of the stage in X-axis direction

J_r	total inertia of rotation components	9.00E-03 [kg · m^2]
B_r	rolling viscosity	6.35E-02 [N · m · s/rad]
M_t	mass of stage	2.73 [kg]
C_t	viscosity between stage and linear guide	1.00E+04 [N · s/m]
K_t	stiffness	1.88E+08 [N/m]
R	conversion ratio	12E-03/2π [m/rad]

Fig. 1. Ball screw driven X-Y stage.

compensation for linear guide friction is also considered to further improve the control performance.

The remainder of this study is organized as follows. Section II described the experimental setup. Section III presents the algorithm to classify the velocity patterns and robust friction compensator based on sinc function is proposed in Section IV. Experiments are performed to show the applicability of the proposed approach in Section V. The conclusion is summarized in Section VI.

2. Ball-screw-driven stage system

2.1 Ball-screw-driven stage Fig. 1 shows the overview of the experimental X–Y ball-screw stage. Each ball screw is directly connected with the shaft of the servo motor through the coupling. The servo motor is equipped with an absolute encoder whose resolution is 2^{20} pulse/rev. Linear scales with a resolution of 100 nm are applied to measure the X,Y-axis positions of the stage. Table. 1 shows the parameters of the stage in X-axis direction. The stage can be model as a two-inertia system whose block diagram is shown in Fig. 2. Here,

ω rotation velocity, [rad/s],
θ rotation angular, [rad],
f_r torque caused by rolling friction, [N · m],
v velocity of stage, [m/s],
x position of stage, [m],
f_l nonlinear friction caused by linear guide, [N],
T motor torque, [N · m].

The rigid-body model of the stage is expressed as follow:

$$P_n(s) := \frac{K_\tau}{Js^2 + Bs}, \quad \cdots\cdots\cdots\cdots\cdots\cdots\cdots\cdots \quad (1)$$

where K_τ is the torque constant, $J := J_r + M_t R^2$ is the nominal inertia and $B := B_r + C_t R^2$ is the nominal viscosity. Fig. 3 shows the frequency response from the current reference to the position of the stage, and the fitted model is shown by the solid line.

The rolling friction characteristics of the stage is shown in Fig. 4 by performing an experiment. It can be observed that the spring-like phenomenon appears at the presliding region $[0, 10]\mu$m.

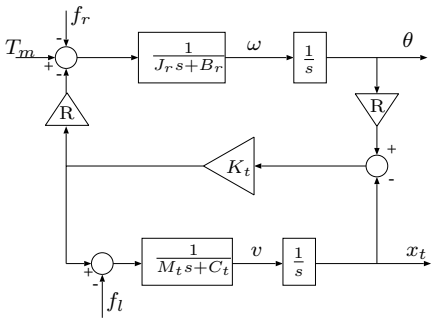

Fig. 2. Block diagram of the system.

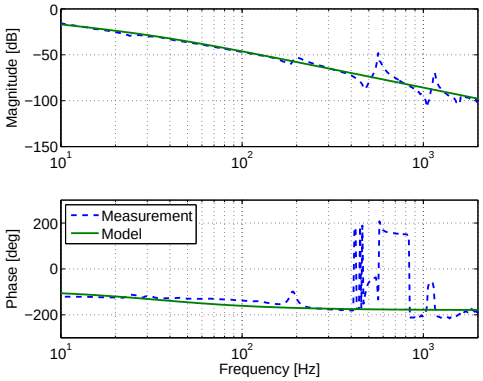

Fig. 3. Frequency response of stage.

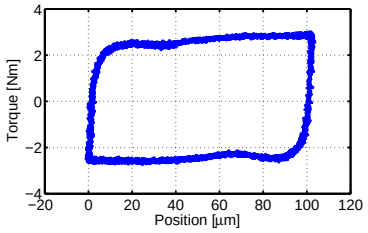

Fig. 4. Rolling friction of the experimental stage.

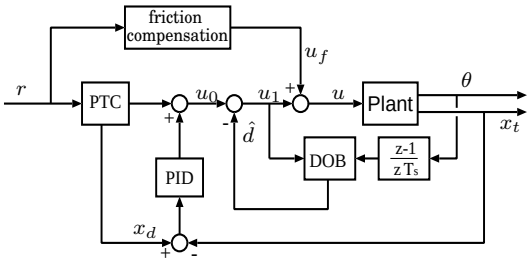

Fig. 5. Block diagram of control system with two-degree-of-freedom controller, an inverse-model-based disturbance observer and feedforward friction compensation.

2.2 Controller design The block diagram of control system is shown in Fig. 5. The feedforward controller is designed as the stable inverse system of the nominal plant via Perfect tracking control (PTC) [1]. The perfect tracking at every sampling instant can be theoretically guaranteed. A PID compensator is applied as the feedback controller,

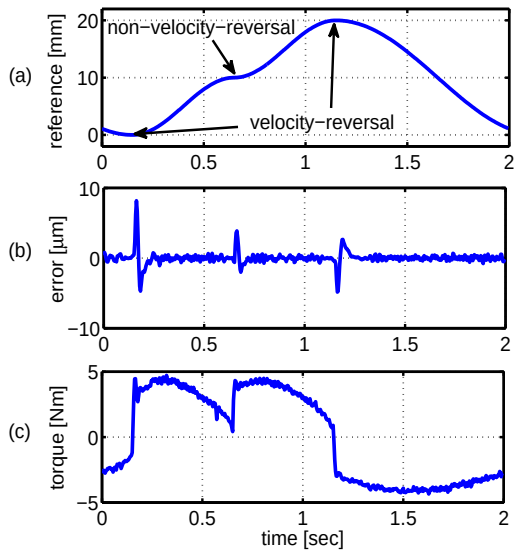

Fig. 6. Experimental results without friction compensation. (a) is the reference, (b) is the position tracking error, and (c) is the input torque.

and the resulting bandwidth of the closed loop is 20 Hz. The stage position x_t The feedforward friction compensation is usually considered, which is also a main topic of this study. An inverse-model-based disturbance observer (DOB) is designed using the motor velocity information [9]. A 1st-order low-pass filter is designed for the disturbance observer with the bandwidth of 80 Hz. DSP(TMS320C6713, 225MHz) is used as the processor to implement the controller. The PID compensator, DOB and friction compensation are discretized by 0.5 ms, and the sampling period for PTC is 1 ms.

Without friction compensation, control performance would be significantly deteriorated at zero velocity. An example is shown in Fig. 6. It is observed that the control accuracy is degraded in both the velocity-reversal case and non-reversal case if friction compensation is not performed. The compensation for the reversal case is actively studied in the literature, however, the study for the non-reversal case is rare as far as the authors know. In the following section, a heuristic method based on sinc function is studied to cope with the situations.

3. Velocity patterns classification and sinc-function-based friction compensation

3.1 Velocity patterns classification Since the friction characteristics is dynamical and highly dependent on the zero-velocity crossing patterns. The algorithm to classify the velocity patterns is firstly studied in this section. For simplicity, the trajectory reference is assumed to be known and it is twice differentiable. In practical situations, this assumption can be generally satisfied.

Denote $r(t)$, $v(t)$ and $a(t)$ as the reference trajectory, velocity and acceleration, respectively. For discrete-time implementation with fixed sampling time, the signals are denoted by r_k, v_k and a_k, where k is the discrete-time index. Define p_k to label the sign of the acceleration a_k by

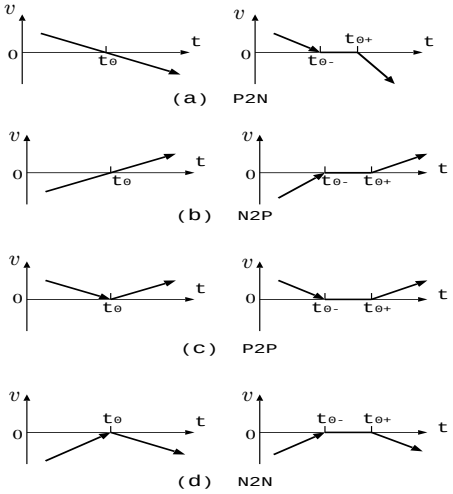

Fig. 7. Classification of velocity patterns in the rolling region.

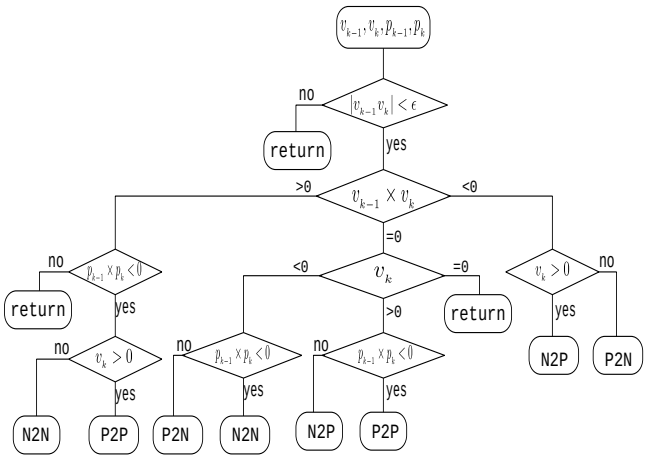

Fig. 8. Algorithm to Classify the velocity patterns in the rolling region.

$$p_k = \begin{cases} 1, & a_k > 0 \\ -1, & a_k < 0 \\ p_{k-1}, & a_k = 0, \end{cases} \quad \cdots\cdots\cdots\cdots\cdots\cdots\cdots\cdots (2)$$

the velocity patterns in zero velocity region can be list as follows according to the sign of the velocity $v(t)$:

- P2N: Positive ⇒ zero ⇒ negative;
- N2P: Negative ⇒ zero ⇒ positive;
- P2P: Positive ⇒ zero ⇒ positive;
- N2N: Negative ⇒ zero ⇒ negative.

Fig. 7 illustrates the velocity patterns at zero velocity. The algorithm to classify these patterns in discrete time is shown in Fig. 8. Here, ϵ is a threshold set as larger than the minimum variation in a sampling period. In the next section, a heuristic method for friction compensation is proposed based on the velocity patterns.

3.2 Sinc-function-based friction compensation Perfect friction compensation requires accurate friction models. However, as introduced in Section I, many of the friction models proposed in the literature are complex and cannot robustly cope with the environment-affected friction. Therefore, a simple friction model which can be real-time tuned

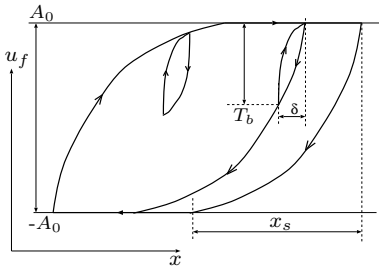

Fig. 9. Rolling friction characteristic.

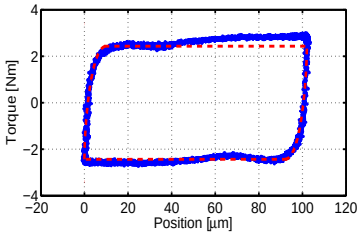

Fig. 10. Comparison of the real rolling friction and sinc function based model.

is of interest. Motivated by this viewpoint and taken the characteristics of ball screw into account, the sinc function is applied in this paper.

The sinc function is defined by

$$y(x) = \mathrm{sinc}(x) := \begin{cases} \frac{\sin(x)}{x}, & x \neq 0 \\ 1, & x = 0 \end{cases} \quad \cdots\cdots\cdots\cdots \quad (3)$$

The Fourier transform of the function is a rectangular function expressed by

$$Y(f) = \begin{cases} 0, & |f| > \frac{\pi}{2} \\ \frac{1}{2}, & |f| = \frac{\pi}{2} \\ 1, & |f| < \frac{\pi}{2}. \end{cases} \quad \cdots\cdots\cdots\cdots\cdots\cdots\cdots \quad (4)$$

Note that the sinc function is the ideal low-pass filter. In the following, a novel friction compensation for ball screw stage based on sinc function is presented.

Consider the N2P case, sinc function applied to fit the rolling friction is expressed by

$$u_{f_a} = \begin{cases} -A_0, & x < 0 \\ 2A_0 \frac{\sin\left(\pi\sqrt{\frac{x}{x_s}} - \pi\right)}{\pi\sqrt{\frac{x}{x_s}} - \pi} - A_0, & 0 \leq x < x_s \\ A_0, & x \geq x_s \end{cases}, \quad (5)$$

where x is the displacement of position from the zero velocity point of N2P case, x_s is the length of the presliding region, and A_0 can be regarded as the Coulomb friction. For the motion in the negative direction, a similar formula can be obtained. Fig. 9 illustrates the rolling friction characteristic. The comparison of the real rolling friction and the sinc-function-based model is shown in Fig. 10, where $x_s = 10\,\mu$m and $A_0 = 2.431\,$Nm. It can be observed that an accurate fitting is achieved.

In the case of reversal motion, the elastic energy in mechanical components are fully excited and released, periodically. The rolling friction varies between $\pm A_0$, and therefore has the potential to be well compensated by properly

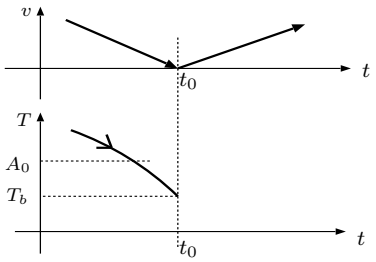

Fig. 11. Illustration of the P2P velocity pattern and the possible trend of the torque.

designed friction models. However, if this is not the case, such as N2N and P2P, the stored elastic energy is not fully released, thus the compensation becomes complex. In the following, sinc function is utilized to perform the compensation. For simplicity, the P2P case is used for analysis.

As the velocity is decelerated to zero, torque is gradually reduced due to the 2-dof controller and the disturbance observer, and the stored energy is partly released. An example is shown in Fig. 6. When the acceleration motion starts, the rolling friction would degrade the control performance. Suppose that the torque is reduced to T_b until the acceleration is start, the released displacement δ can be calculated according to

$$-2A_0 \frac{\sin\left(\pi\sqrt{\frac{\delta}{x_s}} - \pi\right)}{\pi\sqrt{\frac{\delta}{x_s}} - \pi} + A_0 = T_b. \cdots\cdots\cdots\cdots\cdots \quad (6)$$

Newton iteration method can be applied to solve the δ. The details are given in Appendix. When (6) is solved, δ is set as the new length of presliding region. The compensation based on sinc function is given by

$$u_{f_b} = \begin{cases} 0, & y \leq 0 \\ (A_0 - T_b) \frac{\sin\left(\pi\sqrt{\frac{y}{\delta}} - \pi\right)}{\pi\sqrt{\frac{y}{\delta}} - \pi}, & 0 < y < \delta \\ A_0 - T_b, & y \geq \delta \end{cases}, \cdots (7)$$

where y is the displacement of position from the zero velocity point of the P2P case. A similar compensation method can be obtained in the case of N2N pattern.

The friction compensation is realized by $u_f = u_{f_a} + u_{f_b}$. Fig. 12 shows the strategy of friction compensation. In the real situation, the compensation (7) need to be modified for its unnaturalness. The compensation value u_f may be over Coulomb friction A_0 in steady state, as shown by the dotted line in Fig. 12(e). Therefore, the compensation in (7) should return to zero, as shown in (8).

$$u_{f_b} = \begin{cases} 0, & y \leq 0 \\ (A_0 - T_b) \frac{\sin\left(\pi\sqrt{\frac{y}{\delta}} - \pi\right)}{\pi\sqrt{\frac{y}{\delta}} - \pi}, & 0 \leq y < \delta \\ (A_0 - T_b) \frac{\sin\left(\pi\sqrt{\frac{y-\delta}{x_m}}\right)}{\pi\sqrt{\frac{y-\delta}{x_m}}}, & y \geq \delta \end{cases} \cdots (8)$$

x_m should be set sufficiently large to slowly reduce u_{f_b} to zero. In this way, DOB and feedback controller can respond quickly enough to compensate the reduced torque so that the control performance may not be effected. The strategy is shown as the solid line in Fig. 12(d).

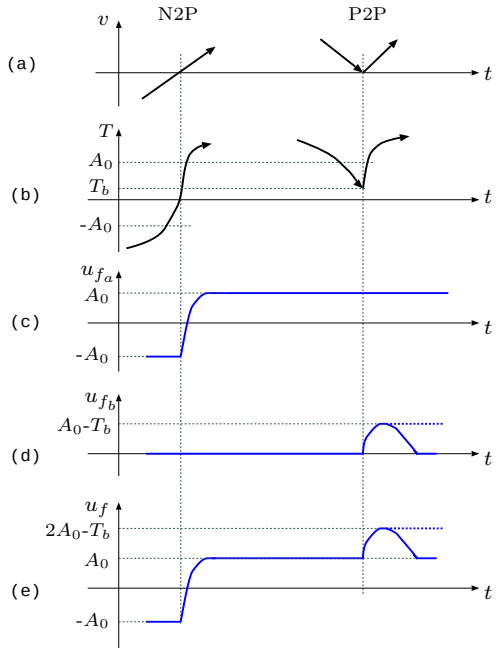

Fig. 12. Illustration of the strategy of the friction compensation. (a) shows the velocity patterns, (b) shows the changing trend of torque, (c), (d) demonstrate the u_{f_a} and u_{f_b}, respectively, and u_f is shown in (e).

4. Experiments

In this section, the sinc-function-based friction compensation method is verified by experiments. Firstly, a sine wave with the magnitude of 10mm is implemented to evaluate the compensation performance of the reversal motion. Two cases that the maximum feed rates are 1 m/min and 5 m/min are considered. Fig. 4 and Fig. 4 show their experimental results. In the figures, (a)s show the reference signal, and the position tracking errors without compensation and with compensation are shown in (b)s. It is observed that the compensation performance was significantly improved by the friction compensation approach. The maximum tracking error is improved from 4.2 μm to 0.92 μm for the first case, and improved from 8.2 μm to 1.98 μm for the second case. The control inputs are shown in (c)s and the compensation torques are shown in (d)s. Thanks to the compensation, the control inputs can respond faster to reduce the effects of rolling friction.

In addition, the compensation effectiveness for the P2P pattern is also evaluated. The experimental results are shown in Fig. 4. Compared with the results shown in Fig. 6, we can see that with compensation, the tracking error can be significantly improved in the P2P case. The tracking error at the P2P region is improved from 3.86 μm to 1.55 μm. Therefore, the effectiveness of the proposed method is verified.

5. Conclusion

In this study, a novel friction compensation method based on velocity pattern recognition and sinc function is discussed. Compared to conventional friction models, the proposed compensation approach can cope with both the reversal motion and non-reversal motion. It also has an advantage that there are only two parameters needed to be identified, namely, the magnitude of Coulomb friction and the length of the spring-like region of ball screws. Therefore, it becomes possible to adjust the parameters in real time according to the working conditions. The proposed approach is also verified by experiments in combination with an inverse-model-based disturbance observer. It is demonstrated that the position tracking performance can be significantly improved in the zero-velocity crossing region.

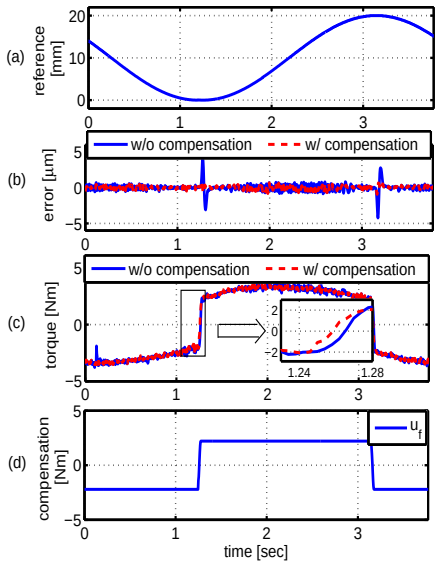

Fig. 13. Experimental results in the case of $v_{\max}$ = 1 m/min.

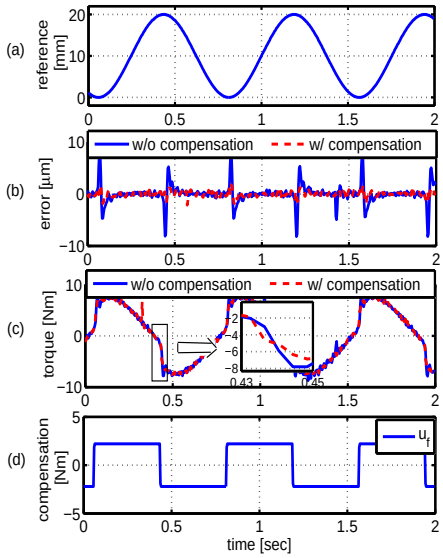

Fig. 14. Experimental results in the case of $v_{\max}$ = 5 m/min.

Appendix

The approach for numerically solving the equation (6): Assume $-A_0 < T_b < A_0$ without loss of generality, and denote

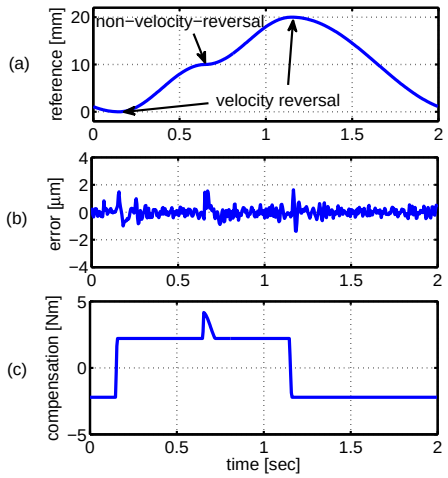

Fig. 15. Experimental results when the reference is irregular.

$$M := \frac{A_0 - T_b}{2A_0}, \quad \cdots\cdots\cdots\cdots\cdots\cdots\cdots\cdots \text{(A1)}$$

$$q := \pi\sqrt{\frac{\delta}{x_s}} - \pi \quad \cdots\cdots\cdots\cdots\cdots\cdots\cdots\cdots \text{(A2)}$$

for the convenience of calculation. It can be obtained that $0 < q < \pi$ since $0 < \delta < x_s$. The equation (6) can be rewritten by

$$\sin q = Mq, \quad 0 < q < \pi. \cdots\cdots\cdots\cdots\cdots\cdots\cdots\cdots \text{(A3)}$$

Define $g(q) = Mq - \sin q$, the equation $g(q) = 0$ can be efficiently solved by mathematical iteration approach, such as Newton iteration method, since $g(q)$ is convex in $0 < q < \pi$ ($g'' > 0$). If q is calculated, δ can be solved according to (A2).

Acknowledgment

This work was supported in part by the MORI SEIKI Co. Ltd.. The authors gratefully acknowledge valuable suggestions from Shinji ISHII, Kouji YAMAMOTO and Yuki TERADA from the MORI SEIKI Co. Ltd..

References

(1) H. Fujimoto, Y. Hori, and A. Kawamura, Perfect Tracking Control based on Multirate Feedforward Control with Generalized Sampling Periods, *IEEE Trans. Ind. Electron.*, vol. 48, No. 3, pp.636-644, 2001.

(2) M. Iwasaki, K. Seki, and Y. Maeda, High-Precision Motion Control Techniques–A Promising Approach to Improving Motion Performance, *IEEE Trans. Ind. Electron. Magazine*, vol. 6, No. 1, pp.32-40, 2012.

(3) H. S. Lee and M. Tomizuka, Robust Motion Controller Design for High-Accuracy Positioning Systems, *IEEE Trans. Indust. Electr.* , Vol. 43, No. 1, pp. 48–55, Feb. 1996.

(4) C. Canudas de Wit, H. Olsson, K. Astrom and P. Lischinsky, A new model for control of systems with friction, *IEEE Trans. Autom. Control*, Vol. 40, No. 5, pp. 419-425, 1995.

(5) F. Al-Bender, V. Lampaert and J. Swevers, The Generalized Maxwell-Slip Model: A Novel Model for Friction Simulation and Compensation, *IEEE Trans. Autom. Control*, Vol. 50, No. 11, pp. 1883-1887, 2005.

(6) P. Dahl, A solid friction model, Aerospace Corp., El Segundo, CA, Tech. Rep. TOR-0158(3107-18), 1968.

(7) J. Swevers, F. Al-Bender, C. G. Ganseman, and T. Prajogo, An integrated friction model structure with improved presliding behavior for accurate friction compensation, *IEEE Trans. Automat. Contr.*, vol. 45, pp. 675–686, Apr. 2000.

(8) S. Sakai and Y. Hori, Ultra-low Speed Control of Servomotor using Low Resolution Rotary Encoder, *in Proc. IECON 21st int. Conf. Ind. Electron.* , Orlando, FL, Vol. 1, pp. 615–620, 1995.

(9) T. Umeno and Y. Hori, Robust Speed Control of DC Servomotors Using Modern Two Degree-of-Freedom Control Design, *IEEE Trans. Indust. Electr.* , Vol. 38, No. 5, pp. 363–368, Oct. 1991.

(10) Z. Jamaludin, H. V. Brussel, and J. Swevers, Friction Compensation of an XY Feed Table Using Friction-Model-Based Feedforward and an Inverse-Model-Based Disturbance Observer, *IEEE Trans. Ind. Electron.* , Vol. 56, No. 10, 2009.

(11) S. Yang and M. Tomizuka, Adaptive Pulse Width Control for Precise Positioning under Influence of Stiction and coulomb Friction, *American Control Conference* , pp. 188–193, Jun. 1987.

(12) H. Asaumi and H. Fujimoto, Proposal on Precise Positioning Control of Ball Screw Stage Based on ITC with PTC, *IEEJ Tech. Rep.*, IIC–07–128, 2007.

(13) M.S. Tsai, M.T. Lin, H.T. Yau, Development of Command-Based Iterative Learning Control Algorithm with Consideration of Friction, Disturbance, and Noise Effects, *IEEE Trans. Control Syst. Technol.*, Vol. 14, No. 3, 2006.